The Effects of Microstructure Heterogeneities and Casting Defects on the Mechanical Properties of High-Pressure Die-Cast AlSi9Cu3(Fe) Alloys

GIULIO TIMELLI and ALBERTO FABRIZI

Detailed investigations of the salient microstructural features and casting defects of the high-pressure die-cast (HPDC) AlSi9Cu3(Fe) alloy are reported. These characteristics are addressed to the mechanical properties and reliability of separate HPDC tensile bars. Metallographic and image analysis techniques have been used to quantitatively examine the microstructural changes throughout the tensile specimen. The results indicate that the die-cast microstructure consists of several microstructural heterogeneities such as positive eutectic segregation bands, externally solidified crystals (ESCs), cold flakes, primary Fe-rich intermetallics (sludge), and porosities. In addition, it results that sludge particles, gas porosity, as well as ESCs, and cold flakes are concentrated toward the casting center while low porosity and fine-grained structure is observed on the surface layer of the castings bars. The local variation of the hardness along the cross section as well as the change of tensile test results as a function of gage diameter of the tensile bars seem to be ascribed to the change of porosity content, eutectic fraction, and amount of sludge. Further, this behavior reflects upon the reliability of the die-cast alloy, as evidenced by the Weibull statistics.

DOI: 10.1007/s11661-014-2515-7

I. INTRODUCTION

ALUMINUM/SILICON alloys are the most commonly diffused foundry alloys in the automotive industry since they respond to the need of decreasing vehicle's weight without compromising strength resistance. A great contribution to the use of Al-Si alloys comes from high-pressure die-casting (HPDC), which allows to increase the production by lowering the cycle time and to manufacture complex-shaped castings with thin wall thickness. Unfortunately, the limit to large diffusion of HPDC remains the final integrity of castings. In HPDC, the metal is injected at high speed into a steel die, thus the associated turbulence represents the major source of inner and surface-casting defects. Further, to be competitive in the market by reducing the cycle time even more, foundries tend to increase the filling velocity, believing that the casting quality will not change. In this way the product requirements will never be satisfied and the amount of scraps increases with a progressive reduction of productive efficiency.

There are several critical features in HPDC, such as forced convection during the filling phase, high speed of molten metal at ingates (up to ~50 ms^{-1}),[1–3] high cooling rate (up to ~10^3 K/s[4,5]), and high pressures (up to ~120 MPa) applied to the biscuit during the intensification stage to assist the feeding of solidification shrinkage in the die cavity.[6,7] All these features produce castings with both microstructures and defects that are markedly different from those created by other foundry processes.

It is widely accepted that a fine-grained, defect-free layer for ms near the casting surface producing a microstructure that is commonly referred to as "the skin" or "the surface layer".[8,9] Furthermore, one of the interesting microstructural characteristics created during HPDC is the narrow bands of positive macrosegregation that commonly follow the contour of components.[10] The central region of die-castings, or *core*, contains a mixture of fine grains and externally solidified crystals (ESCs), which mainly form in the shot sleeve and are injected into the die cavity during die filling.[11,12] Generally, this region is also characterized by great amount of casting defects, such as porosity,[7,13] which have deleterious effects on the mechanical properties of die-castings.[14] In addition, the core also shows a large fraction of coarse intermetallic compounds containing Fe, Mn, and Cr, which are present as impurity elements in recycled Al foundry alloys, such as AlSi9Cu3(Fe) alloys.[15] The formation of these crystals, also named *sludge*, can occur throughout the HPDC process, such as in the holding furnace, in the ladle (or feed pipe) during the melt transfer to cold chamber die-casting machine, or inside the shot sleeve before the plunger moves forward.[15]

A good interpretation of the characteristic defects and microstructural features in HPDC, and their impact on the mechanical behavior of die-cast components are fundamental for developing improved castings. This is

GIULIO TIMELLI, Assistant Professor, and ALBERTO FABRIZI, Postdoctoral Student, are with the Department of Management and Engineering, University of Padova, Stradella S. Nicola, 3, 36100, Vicenza, Italy. Contact e-mail: timelli@gest.unipd.it
Manuscript submitted January 24, 2014.
Article published online August 15, 2014

especially critical for structural HPDC components, where safety and reliability are key requirements.

In the present work, some of the salient microstructural heterogeneities in HPDC, such as defect bands, ESCs, cold flakes, surface skin and sludge segregation, and casting defects, *i.e.*, gas porosity, are examined in detail for a high-pressure die-cast AlSi9Cu3(Fe) alloy. These features are then addressed to the mechanical properties and the reliability of separately die-cast tensile bars, which is estimated by a Weibull statistical approach. A hypoeutectic Al-Si-Cu alloy, AlSi9Cu3(Fe) (EN AB-46000), which is among the most common die-casting alloy in Europe,[16] was used in this study.

II. EXPERIMENTAL PROCEDURE

A. *Alloy and Casting Procedure*

In the present work, the AlSi9Cu3(Fe) foundry alloy (EN AB-46000, equivalent to the US designation A380[17]) was produced by Raffineria Metalli Capra through aluminum scrap recovered from industrial waste and discarded post-consumer items. The treatment of the scrap to produce new aluminum metal and alloys is known as recycling, and metal produced in this way is frequently termed *secondary*.[18]

The alloy, supplied here as commercial ingots and referred to a single production batch, was melted in a 300 kg SiC crucible in a gas-fired furnace set up at 1073 K ± 10 K (800 °C ± 10 °C) and maintained at this temperature for at least 3 hours. The temperature of the melt was then gradually decreased by following the furnace inertia up to 963 K ± 5 K (690 °C ± 5 °C). The hydrogen content of the melt in the holding furnace was analyzed by Foseco ALSPEK H® analyzer, and it was almost constant at 0.22 mL/100 g Al during the entire experimental campaign. Periodically, the molten metal was manually skimmed with a coated paddle. The chemical composition, measured by optical emission spectrometry, is shown in Table I.

Casting was carried out in an Italpresse 2.9 MN locking force cold-chamber HPDC machine, and a multicavity die was used to produce high-pressure die-cast specimens with geometry shown in Figure 1. A more detailed description of the HPDC machine, the casting procedure, and all the process parameters is given elsewhere.[15,19] The die-castings have been stored at room temperature for about 5 months before being analyzed and were, therefore, similar to a T1-condition. Generally, this temper designation applies to products that are cooled from an elevated-temperature shaping process, like HPDC, and for which mechanical properties have been stabilized by room temperature aging.

B. *Microstructural Characterization*

This study only examined round tensile specimens from the position indicated in Figure 1, and whose dimensions are shown in Figure 2. The samples cut from the cross section of the gage length were mechanically prepared to a 3-μm finish with diamond paste and, finally, polished with a commercial fine silica slurry for metallographic investigations. Microstructural analysis was carried out using an optical microscope (OM) and a field emission gun-environmental scanning electron microscope (FEG-ESEM) equipped with an energy-dispersive spectrometer (EDS), and quantitatively analyzed using an image analyzer.

The area fraction and distribution of primary Fe-bearing compounds were investigated and measured in the entire cross section of tensile specimens. Other intermetallic phases, such as $CuAl_2$ particles, were excluded from the measurements. Furthermore, to quantitatively calculate the eutectic area fraction, the polished specimens were previously etched in a modified Murakami etchant (60 mL H_2O, 10 g NaOH, and 5 g $K_3Fe(CN)_6$). At low magnification, the α-Al phase and the Al-Si eutectic and intermetallics appeared white and black, respectively, and, therefore, distinguishable by quantitative metallography software.

To evaluate the grain structure, electron back-scatter diffraction (EBSD) investigations were performed on the sample surfaces polished by ion milling.

C. *Porosity Investigation*

A quantitative evaluation of porosity content was carried out by means of density measurements. Specimens drawn from the gage section of tensile specimens were weighted in air and water, and the density ρ calculated according to Archimedes's principle:

$$\frac{W_a}{W_a - W_o}\rho_0 = \rho, \qquad [1]$$

where W_a and W_o are the weights in air and water, and ρ_0 the density of water at room. The porosity content is then defined as:

$$\text{Porosity} = \frac{\rho_{nom} - \rho}{\rho_{nom}}, \qquad [2]$$

where ρ_{nom} is the density of fully dense material, which is here assumed to be 2.770 g/cm^3 as indicated in Reference 20.

In order to detect the hydrogen level entrapped in the casting, specimens with a weight of about 3 g were drawn from the region of the biscuit and from the tensile grip section closer to the ingate, and analyzed by LECO® method. This technique is based on the fusion of a sample inside a graphite crucible at a temperature

Table I. Chemical Composition of the Experimental Alloy (Weight Percent)

Si	Fe	Cu	Mg	Mn	Zn	Cr	Ni	Pb	Bi	Al
8.314	0.793	2.846	0.251	0.257	0.897	0.080	0.081	0.083	0.013	bal.

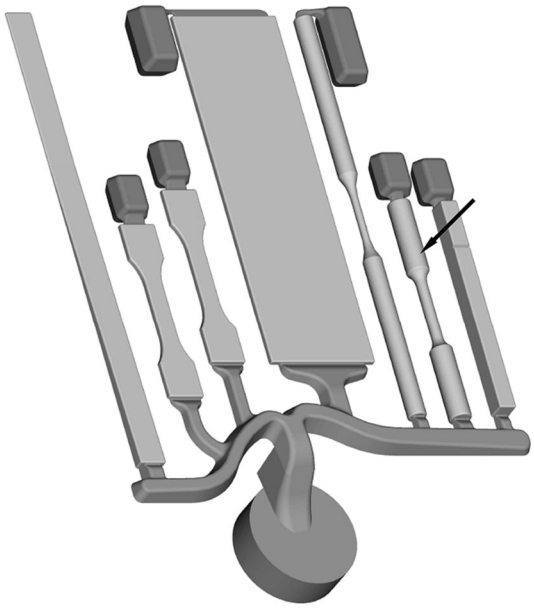

Fig. 1—Geometry of the die-casting where the investigated round tensile bar is indicated by arrow.

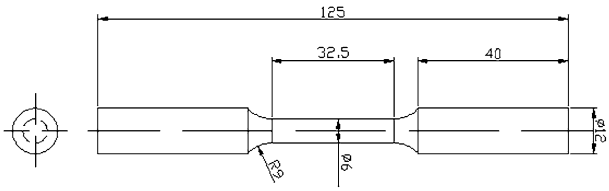

Fig. 2—Geometry of die-cast tensile test specimen (mm).

above the melting point within an inert gas such as argon. Subsequently the thermal conductivity method is used for the measurement of evolved hydrogen.

D. *Mechanical Testing*

Hardness measurements were performed on ground and polished samples drawn from the gage sections of round tensile bars. Vickers microhardness measurements were carried out using a load of 0.1 kgf and a 30 seconds dwell period, according to the standard ASTM E384-11e1[21]; forty indentations were performed along the cross section of the samples. In order to describe the effect of microstructural variations on the tensile properties over the sample diameter, tensile bars were also machined along the gage section to obtain different bearing areas. Therefore, the analyzed tensile bars presented a gage diameter of 6.0, 3.4, and 3.0 mm, respectively.

At least seven tensile tests were done for each gage diameter on a MTS 809 tensile testing machine according to the UNI EN ISO 6892-1:2009.[22] The crosshead speed was 2 mm/min and the strain was measured using a 25-mm extensometer. Experimental data were collected and processed to provide yield stress (YS, actually 0.2 pct proof stress), ultimate tensile strength (UTS),

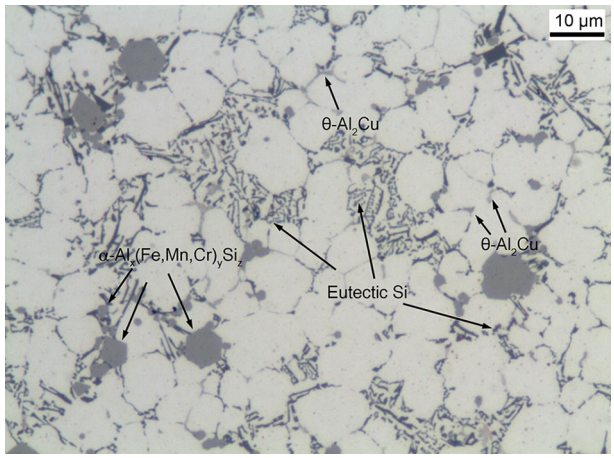

Fig. 3—Microstructure of die-cast AlSi9Cu3(Fe) alloy, as observed at the center of the round tensile bar.

elongation to fracture (s_f), and quality index Q, which takes into account the UTS and s_f in the equation[23]:

$$Q = \mathrm{UTS} + 0.4K\ \log(s_f), \qquad [3]$$

where K is the material's strength coefficient.

The two-parameter Weibull analysis was applied to accurately describe the distribution of tensile properties.[24,25] The slope of the linearized Weibull plot, known as Weibull modulus, represents an index of the reliability of the experimental data. According to Green *et al.*,[26] this parameter seems to be more important than the average mechanical properties.

III. RESULTS AND DISCUSSION

A. *General Microstructure*

The microstructure of the die-cast AlSi9Cu3(Fe) alloy mainly consists of a primary phase, α-Al solid solution, and an eutectic mixture of aluminum and silicon (Figure 3). The α-Al phase precipitates from the liquid in the form of equiaxed and less-branched dendrites. This morphology is probably due to the high cooling rate and intense shear in the die cavity during HPDC; it is well known how the nucleation prevails on the growing mechanism due to higher undercooling. Therefore, due to reduced space, α-Al crystals are prevented from growing and forming well-defined dendrites before impinging each other. Further, the intense shear during solidification interferes with the dendritic growing mechanism of solidifying α-Al crystals.[27]

The eutectic Si shows a coarse plate-like morphology at the center of the tensile specimen, typical of unmodified Al-Si alloys (Figure 3), while fine and fibrous eutectic Si particles are contrary revealed at the casting surface due to higher cooling rate, as also reported elsewhere,[15] Thus, it is established that rapid solidification process changes the eutectic Si shape so that it is similar to chemically modified eutectic Si.[28]

Intermetallic compounds, such as Cu- and Fe-rich intermetallics, are also observed in the interdendritic

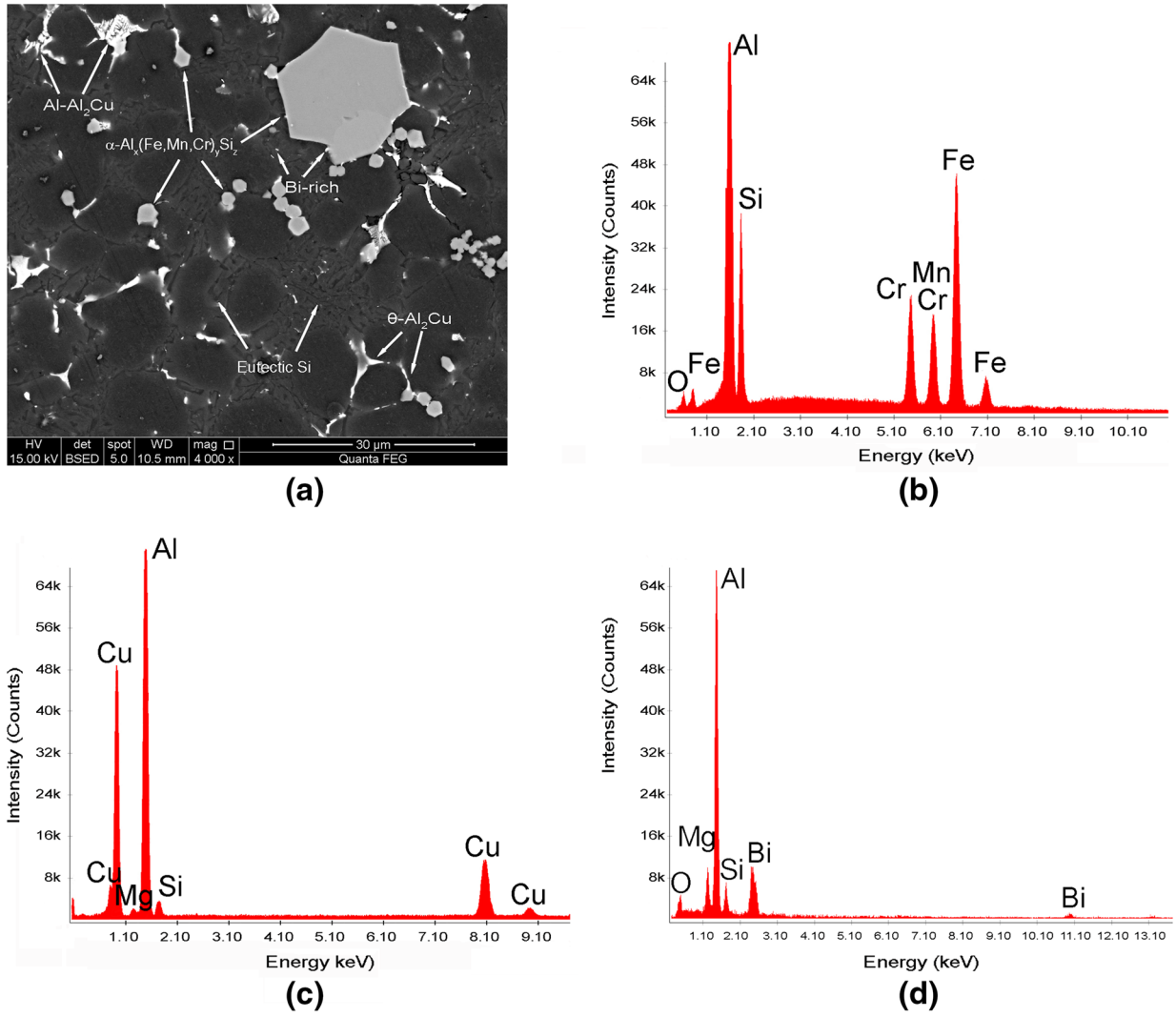

Fig. 4—(*a*) Backscattered SEM micrograph of die-cast AlSi9Cu3(Fe) alloy. Arrows indicate α-$Al_x(Fe,Mn,Cr)_ySi_z$ compounds, Cu- and Bi-rich particles, as revealed by (*b*) through (*d*) EDS spectra, respectively. Clustering of secondary Fe-rich particles is visible in the micrograph.

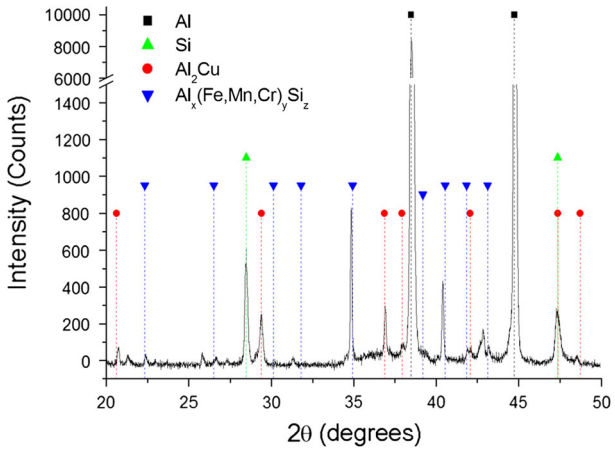

Fig. 5—XRD spectrum of die-cast AlSi9Cu3(Fe) alloy.

region and along the grain boundaries (Figures 3 and 4). The Cu-bearing particles were identified as θ-Al_2Cu phase that occurs both in the form of pockets of fine eutectic (Al + Al_2Cu) in the interdendritic regions and blocky-like Al_2Cu particles (Figure 4). The former is due to high cooling rate in HPDC, while the latter is consequence of high fraction of Fe-rich intermetallics, nucleating site for Al_2Cu.

Blocky-like α-$Al_x(Fe,Mn,Cr)_ySi_z$ particles, as revealed by EDS and XRD investigations (see Figures 4 and 5), show a dimension ranging from few microns to a size comparable to the α-Al cell. While the firsts are referred to proeutectic (or *secondary*) intermetallic compounds, the coarser particles are usually called *sludge*.

Fine Bi-rich particles, as revealed by the EDS analysis (Figure 4(c)), are also present in the interdendritic regions and along grain boundaries. Due to high solidification rate and very low Bi solubility in α-Al phase, these particles are in the size range of few μm and can show rod-type or blocky morphologies, as reported elsewhere.[29]

In Figure 5, the XRD spectrum of the die-cast AlSi9Cu3(Fe) alloy is reported. Besides Al and Si phases, the measurements evidence the presence of more

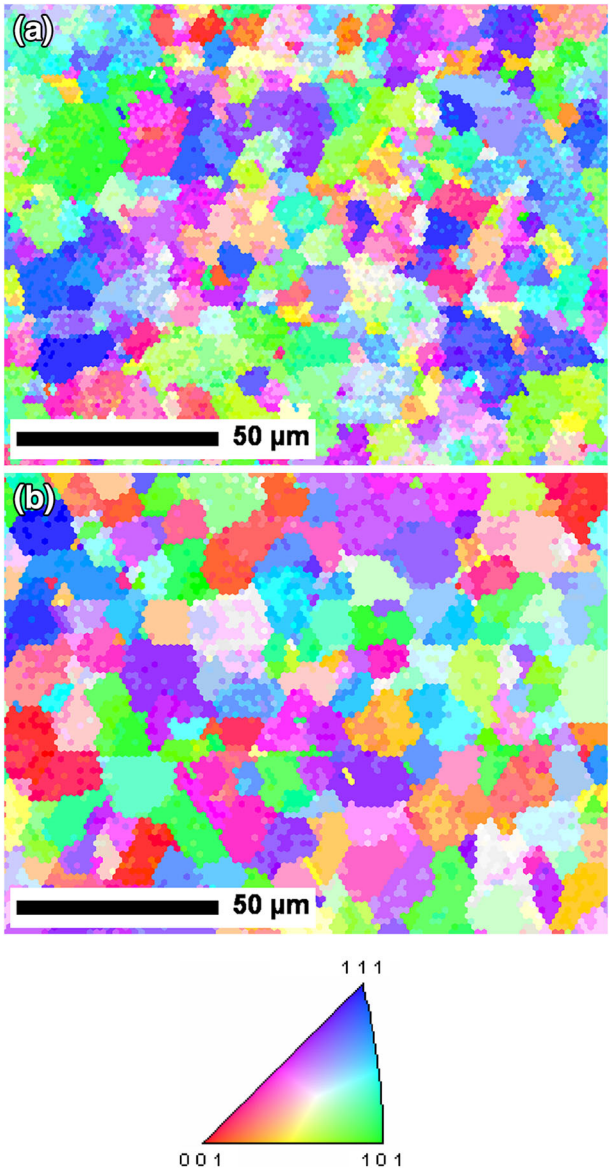

Fig. 6—EBSD orientation maps obtained (a) near the surface and (b) in the central cross section of the tensile bars (Color figure online).

frequent intermetallic compounds such as θ-Al_2Cu and cubic α-$Al_x(Fe,Mn,Cr)_ySi_z$ phases. The obtained diffraction peaks were successfully compared with the JCPDS card N. 25-0012 in order to recognize the tetragonal θ-Al_2Cu phase whereas, the identification of bcc α-$Al_x(Fe,Mn,Cr)_ySi_z$ phase was supported by literature data.[30,31]

B. *Grain Size Analysis*

The grain structure was evaluated at the center and near the casting surface of tensile bars by means of EBSD analysis. Typical EBSD grain-orientation maps for the different regions are shown in Figure 6. From the EBSD images, it appears that the alloy shows an equiaxed structure with no texture or preferential grain orientation in the specimens. Further, the EBSD results

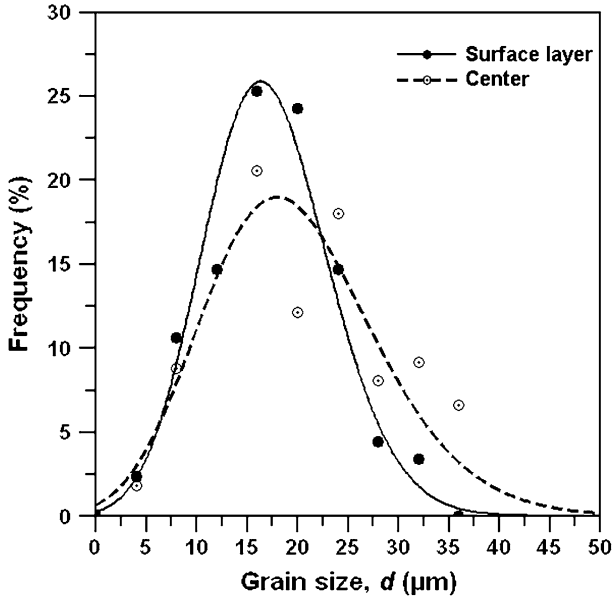

Fig. 7—Grain-size distributions with the associated log-normal fit curves obtained near the surface and at the central cross section of the tensile bars.

allowed to evaluate the grain size (d) distribution. Figure 7 shows that the equiaxed grains are size-distributed according to a log-normal distribution and the average grain values are 20.2 ± 8.6 and 17.1 ± 6.2 μm at the center and near the casting surface, respectively. By moving to the core of the tensile bars, the distribution of the grain size becomes more spread. The grain size with the maximum frequency shifts to higher d values and the absolute value of the maximum frequency decreases. Despite the relatively low content of ESCs in the analyzed specimens (further discussed in Section III–C–2), their segregation toward the central regions can be referred as the reason of higher average value and standard deviation of grain size. By excluding ESC populations from grain size measurement in similar tensile bars, it has been recently demonstrated how the average grain size of *in-cavity* solidified grains is almost uniform over the cross section, with, however, finer grains on the casting surface.[13] In the present work, the ESCs were not excluded from the measurement.

C. *Microstructural Heterogeneities*

1. *Defect band*

Figure 8(a) shows a typical etched macrostructure of the gage section of die-cast AlSi9Cu3(Fe) tensile bars. A dark band of positive segregation follows the contour of the casting surface. This microstructural feature, commonly called *defect band* or *segregation band*, is typically observed in Al-Si die-castings[7,10,13] and it generally contains a higher volume fraction of eutectic than the surrounding material. Gourlay and Dahle[32] and Meylan *et al.*[33] explained how defect bands form from the expansion of a sheared network of solid crystals. This expansion has been interpreted according to the Reynolds' dilatancy, which typically occurs in compacted

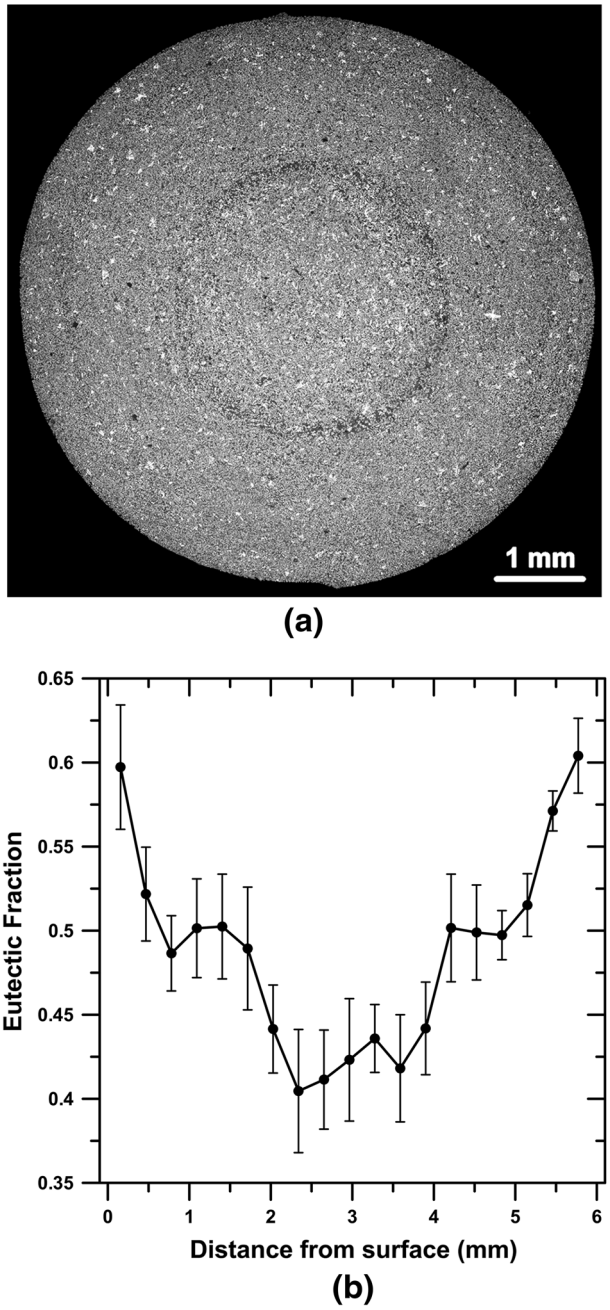

Fig. 8—(*a*) Etched cross section of die-cast AlSi9Cu3(Fe) tensile specimen; darker regions in the macrograph contains higher fraction of Al-Si eutectic and intermetallics. (*b*) Mean eutectic profile over the entire cross section of the analyzed alloy; the scattering of data is depicted by vertical bars.

granular materials, or concentrated suspensions, when the particles are so constricted that they must be pushed apart for the material to change shape by particle rearrangement. The dilatant deformation due to rearrangement leads to the formation of local shear bands, where enriched solute liquid flows into, resulting in positive macrosegregation. In die-cast Al-Si-Cu alloys, these conditions are verified due to a combination of small grain size (~10 μm), relatively unbranched equiaxed crystal shape, and the significant shear stresses (≤100 MPa) that act during HPDC.

Due to the short freezing range and great eutectic fraction of AlSi9Cu3(Fe) alloys, the defect band does not contain a significant level of porosity that is typical for HPDC Mg alloys.[10] On the contrary, higher solute content than the average alloy composition (*positive macrosegregation*) is contained, as described in detail in References 7, 13, 34, 35.

The cross section shown in Figure 8(a) was used to determine the local eutectic variations over the cross section of die-cast sample. Each data point in Figure 8(b) represents the eutectic fraction in an area 312 × 232 μm^2, and it was obtained from micrographs taken at 300 μm intervals by approximating the eutectic fraction as the area fraction of black in each micrograph. In the analyzed alloys, the total area fraction of Fe-bearing intermetallics was estimated to be less than ~3 pct, while the fraction of Cu-rich phases was less than 2 pct; therefore, these phases make only a small contribution to the area fraction of eutectic. At least four profiles traversing through the casting center were measured and subsequently averaged. The eutectic profile quantitatively evidences how the defect band is located in the region of ~1.6 mm from the surface of the bar and the average thickness of the segregation band is 246 ± 60 μm, where the high standard deviation is explained by the high Si content, which makes broad and blurry band.[35] A comparison of band location and thickness in similar die-cast AlSi4MgMn and AlSi7MgMn tensile bars[10,13,34] reveals how the defect band moves toward the casting surface and increases in thickness by increasing Si content. Recently, Otarawanna *et al.*[34] revealed how the band thickness is generally in the range between 7 and 18 mean grains wide, independently of Al or Mg alloy.

From the microstructural investigations, it is revealed that how multiple macrosegregations exist in the analyzed AlSi9Cu3(Fe) specimens. The macrosegregation profile consists of at least two other components, besides the aforementioned *defect band*: (a) a macrosegregation in the casting surface and (b) a general eutectic increase from the casting center to the surface. It was proposed that both phenomena are strictly connected and result from a combination of inverse segregation and exudation.[36,37]

Detailed micrographs of the die-cast AlSi9Cu3(Fe) alloy are also shown in Figure 9; these refer to the casting surface, the region of the defect band and the center of the round tensile bars, respectively.

2. *Externally solidified crystals and cold flakes*

Large bright α-Al crystals, visible in Figure 9, can be observed in a matrix of fine globular-rosette in-cavity solidified grains. Such crystals, generally known as externally solidified crystals, mainly form in the shot sleeve or during the melt transfer from the holding furnace to the shot sleeve, and they are injected into the die cavity during die filling.[11,12] Optical observation indicates that the total fraction of ESCs is relatively low (less than 5 pct). ESCs with both branched-dendritic

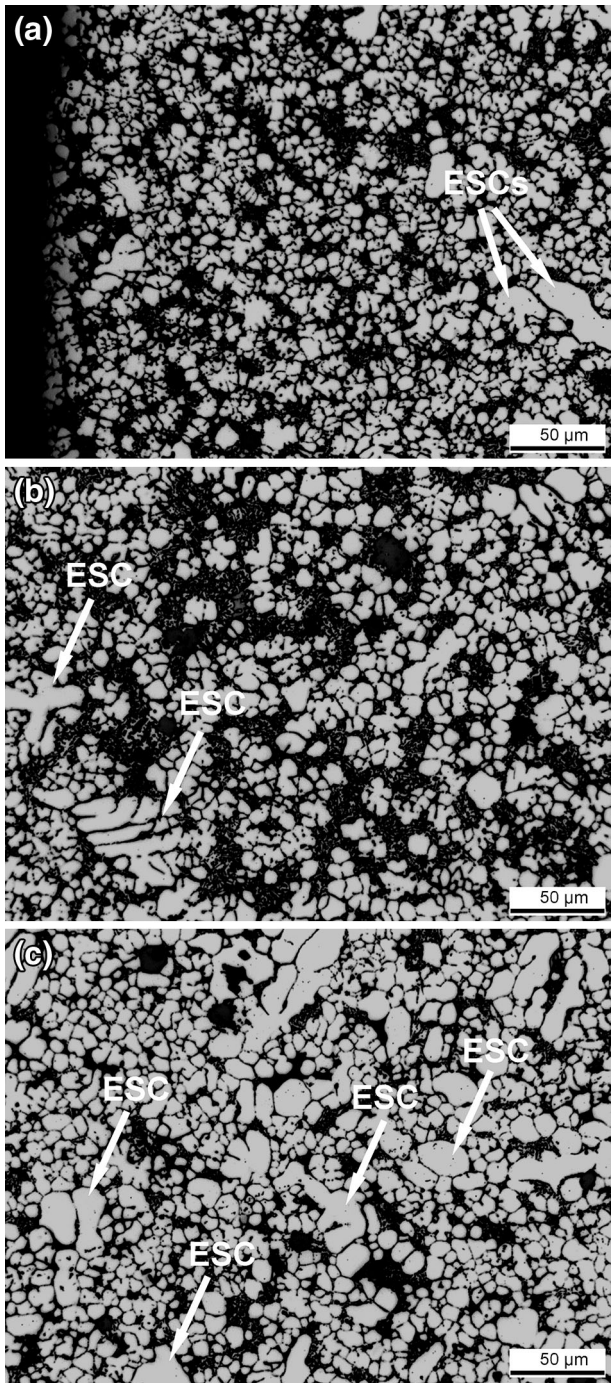

Fig. 9—Typical etched microstructures from (*a*) the casting surface, (*b*) within the defect band, and (*c*) the center of the casting. The α-Al grains appear bright, while Al-Si eutectic and secondary intermetallics appear dark. ESCs are indicated with arrows.

and globular-rosette morphology are present in the samples (see Figure 9).

The ESCs differ from *cold flakes*, which are occasionally observed in the cross section of tensile bars (Figure 10). Cold flakes form due to the breaking up of the solid layer at the shot sleeve wall by the movement of the plunger and are entrapped into the die cavity during die filling as inclusion of several millimeters in size.[38]

Both ESCs and cold flakes are mainly concentrated toward the casting center, in a region defined by the defect band. This behavior can be explained considering that a solidifying surface layer forms during filling of the die cavity, and it constricts the metal to flow in the centerline of casting. Another factor to be considered is the die temperature, which affects the degree of metal-die flow constraint.[12]

3. *Surface layer*

In die-cast components, it frequently reported the presence of a skin layer of several hundred micrometers thick with different microstructures from the adjacent regions, free of porosity and harder than more central region. In the present work, no distinctive microstructural layer is revealed at the casting surface of the die-cast AlSi9Cu3(Fe) specimens, therefore, it was not possible to define a *skin* from the microstructural observations. The absence of a skin could be explained considering the liquid flow in the die cavity of the tensile bar. The injected metal is likely to impinge the die surface during die filling with high velocity and pressure producing great heat transfer from the alloy to the die. Thus, solidification can occur but any crystals that form are swept away by the filling flow. Therefore, along the gage length, microstructure formation begins after the filling velocity has slowed or stopped.

Furthermore, there exists a *surface layer* of about 1.3-mm thick in the analyzed tensile bars that is free of porosity, and with few entrapped ESCs and primary coarse Fe-rich compounds. This surface layer is marked by the defect band and could be referred to as the skin in this study, in accordance with.[39]

4. *Sludge segregation*

Large blocky-like α-$Al_x(Fe,Mn,Cr)_ySi_z$ particles, as revealed by the EDS analysis (see Figure 4), are observed in the microstructure (Figure 3). Comparison of the particle size to the α-Al cell size of the alloy reveals that these particles are primary phases. These complex intermetallic compounds are usually called *sludge*. In secondary Al alloys with high Si content, α-$Al_x(Fe,Mn,Cr)_ySi_z$ phase may be primary, and since the crystals tend to be limited by the (111) faces, they appear as more or less well-formed hexagons.[30] In the present work, the relatively high cooling rate prevented the formation of primary Chinese script and large needle-like sludge particles. Shabestari[30] and Warmuzeka *et al.*[40] demonstrated how the stoichiometry and the crystal structure of sludge particles is α(bcc) [$(Al_{12}(Fe,Mn,Cr)_3Si_2)$].

While the total area fraction of Fe-bearing intermetallics was measured to be up to 3.0 pct in the analyzed alloy, the average fraction of sludge compounds (particles coarser than 10 μm^2) is about 0.6 pct. It was proposed that, when the temperature in the holding furnace is sufficiently high [*e.g.*, ≥963 K (690 °C)], sludge particles can form in cold-chamber HPDC during the transport of molten metal from the casting furnace

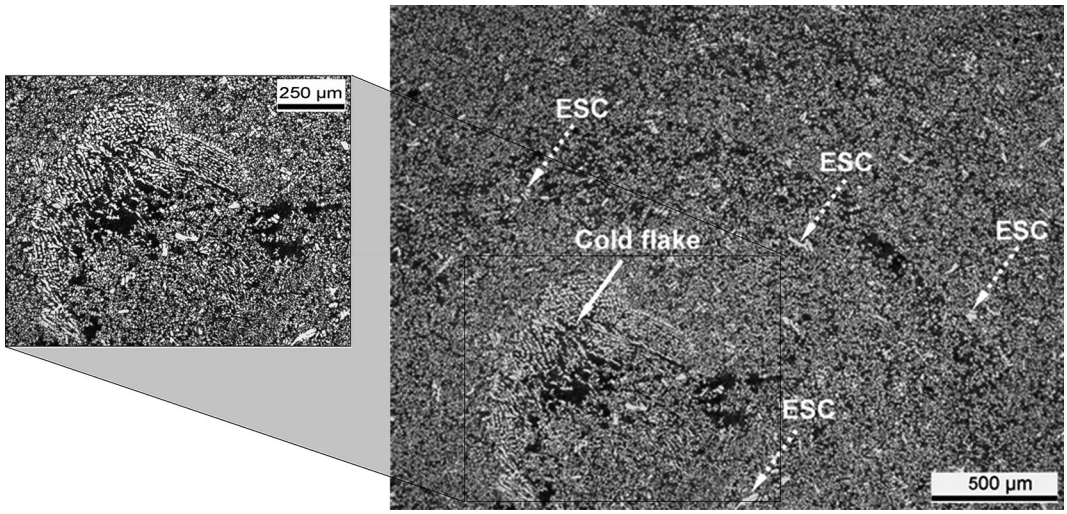

Fig. 10—Etched microstructure obtained at the center of the tensile bar. The core of the specimen is defined by a visible eutectic segregation band. ESCs and cold flake, also shown in the insert, are indicated by arrows.

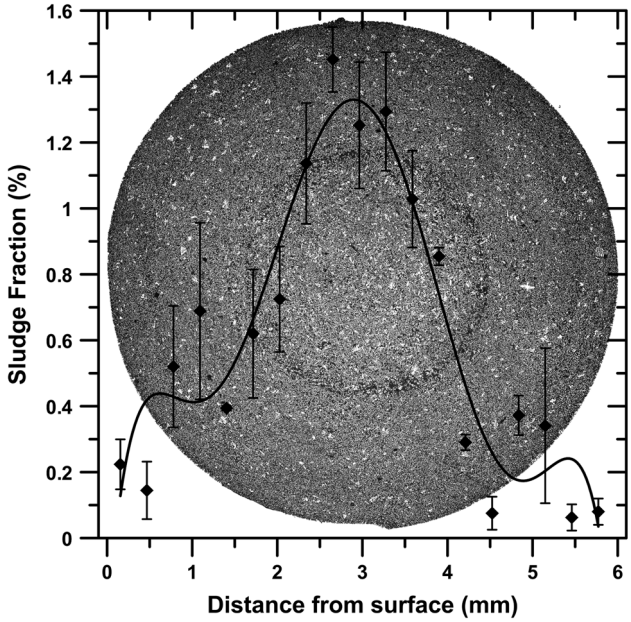

Fig. 11—Mean sludge profile over the cross section of die-cast Al-Si9Cu3(Fe) tensile specimen. Particles with size higher than 10 μm^2 were considered.

to the shot sleeve and inside the cold chamber, as well as ESCs.[15] The crystals are then transported into the liquid by the flow of melt during filling, and they survive as the melt is sufficiently cold.

The local sludge variation was studied over the cross section of tensile bars (Figure 11) using a similar procedure for local eutectic analysis. These primary compounds tend to accumulate in the central region of the samples, whereas the surface layer shows few sludge crystals. Furthermore, the amount of sludge was also estimated along the longitudinal direction of the tensile bar, and it results that the sludge content decreases with distance from the ingate (Figure 12); a quantitative investigation of this behavior was carried out and described in detail elsewhere.[41] Such segregation mechanism is similar to that suggested for the ESCs entrapment.[12]

D. *Porosity Characterization*

The tensile specimens were machined in order to remove firstly the surface layer (Ø3.4) and then the defect band region (Ø3.0). The density and porosity content in the gage section of die-cast (Ø6.0) and machined tensile bars (Ø3.4 and Ø3.0) are shown in Figure 13. In general, the die-cast tensile specimens show a good integrity level; this is reasonable to expect from their geometry and the process parameters used. Reducing the gage section, the density decreases from 2.758 to 2.690 g/cm^3, and the porosity content, calculated according to Eq. [2], increases. Therefore, porosity tends to be located toward the center of the cross section, enclosed by the inner defect band, whereas the surface layer contains little porosity. This is also evidenced in the macrograph of Figure 14. The alloy in contact with the die solidifies relatively and rapidly and is fed from the hottest central region of the gage section, resulting in little shrinkage porosity. Additionally, the solidifying surface layer constricts the metal to flow toward the centerline of casting, thus forcing the air/gas entrapment porosity too. Recently, it was observed how the volume fraction of pores in similar tensile bars is substantially higher in the grip sections than in the gage section[13,15] and, in particular, close to the overflows (see Figure 12) where air/gas bubbles can be entrapped during the die filling phase.

The total porosity in the tensile bar is the contribution of alloy solidification shrinkage and gas entrapment. Considering the geometry of the tensile specimen, high cooling rate is obtained in the gage section than in the grip sections due to a significant difference in the volume to surface ratio. The gage section is expected to be fed from the material with lower fraction solid, *i.e.*, the grip sections. Thus, the formation of porosity due to

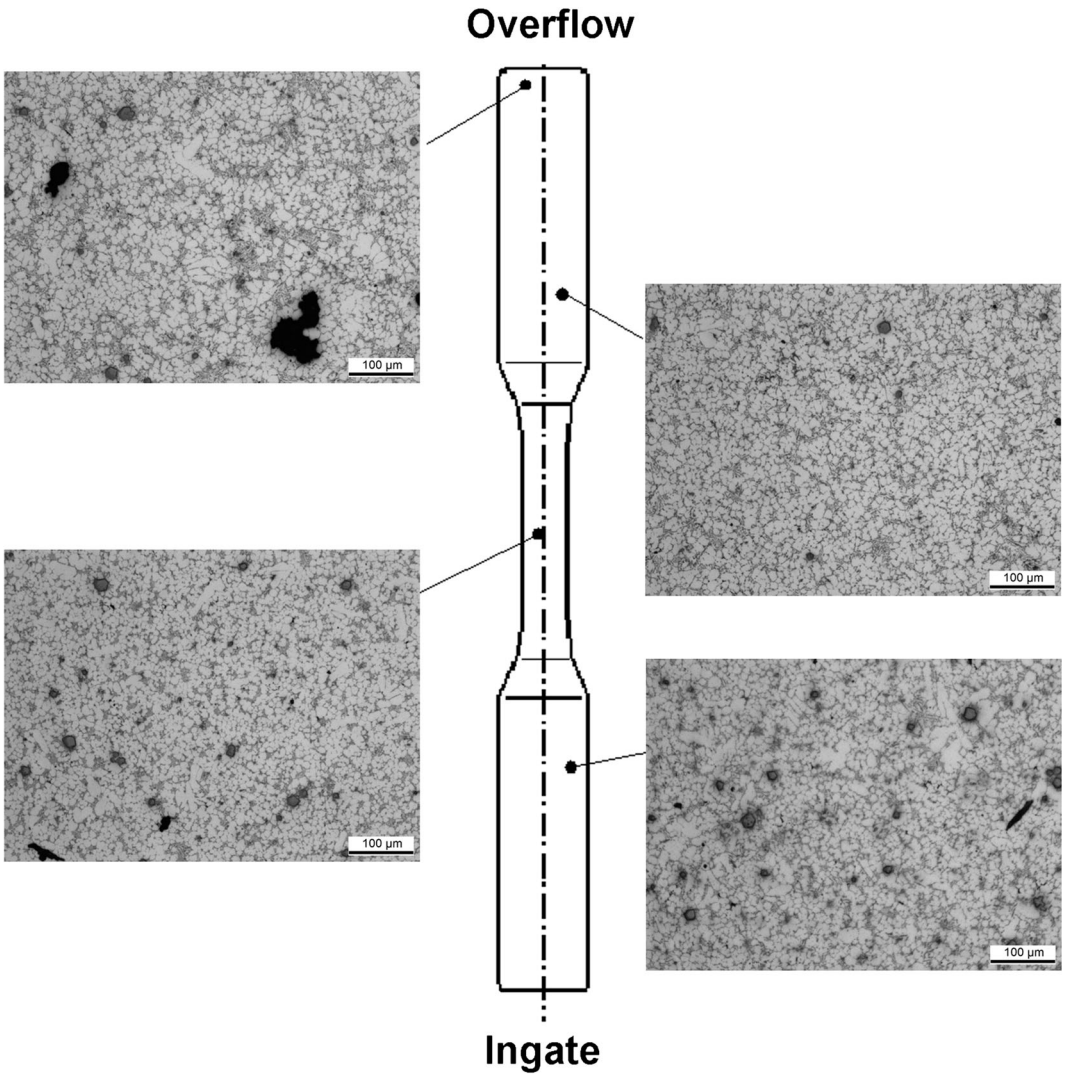

Fig. 12—Typical microstructures along die-cast AlSi9Cu3(Fe) tensile bar. Large blocky-like crystals are sludge particles.

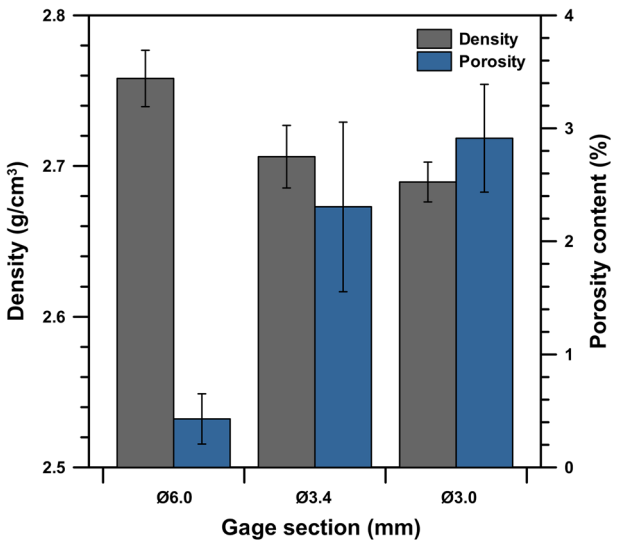

Fig. 13—Density and porosity content measured in the gage section of die-cast (Ø6.0) and machined tensile bars (Ø3.4 and Ø3.0). The standard deviations are given as error bars.

shrinkage is reduced in the gage section by the provision of feed liquid from the grips.

On the other hand, the total porosity due to gas entrapment (v in mL/100 g Al) includes gas from physical entrapment (v_{entrap}), gas from lubricant decomposition (v_{lubr}), and gas initially dissolved in the alloy ($v_{soluble}$) according to[42]

$$v = v_{entrap} + v_{lubr} + v_{soluble} \quad [4]$$

As aforementioned, the dissolved hydrogen level in the melt in the holding furnace was evaluated almost steady at 0.22 mL/100 g Al during the HPDC experiments, while the final hydrogen content in the casting is reported in Table II. Firstly, it is evident how the gas content is not uniformly distributed in the die-casting, with higher values in the round tensile specimen than in the region of the biscuit. Further, the hydrogen values measured in the castings by LECO® method are significantly higher than the initial hydrogen dissolved in the bath. Therefore, the gas component given by gases from physical entrapment and lubricant decomposition is predominant.

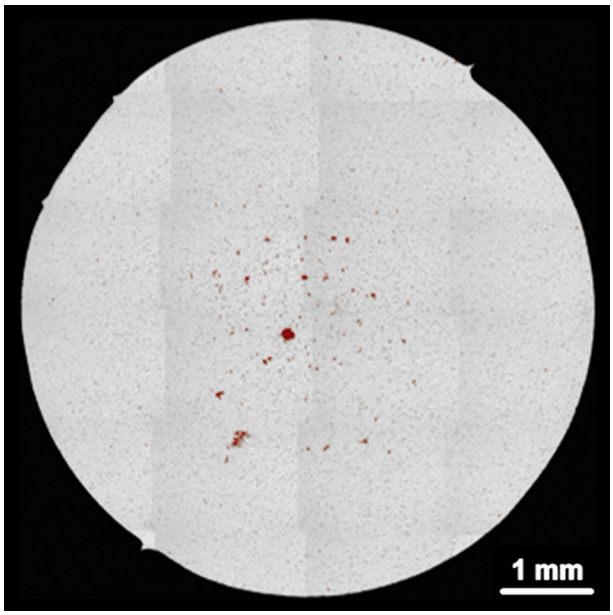

Fig. 14—Macrograph taken from the gage section of die-cast tensile bar showing porosity distribution. Pores are highlighted in red. The picture refers to a tensile specimen intentionally selected with higher porosity content than standard produced bars (Color figure online).

Table II. Hydrogen Content Measured in the Region of the Biscuit and in the Tensile Grip Section Closer to the Ingate

Analyzed Region	Hydrogen Content (mL/100 g Al)
Biscuit	0.88 (0.33)
Grip section	1.13 (0.43)

Standard deviation in parentheses.

Generally, the gas porosity due to dissolved hydrogen is not common in HPDC, where the contributions to gas pores' formation is mainly due to the decomposition of coolant and die lubrication.[42] Normally, the die cavity and plunger tip are sprayed with a water-based oil or lubricant. This increases the die material life and reduces the adhesion of the solidified component. However, as liquid metal is injected into the die, the lubricant, especially if water-based, will boil. If there is no route for the vapor to escape through the overflows, it may be entrapped into the liquid metal as bubbles, which are dragged inside the die cavity. Typically, water-based lubricants are sprayed onto the surface of the die between metal injections, while powder lubricants are used in the shot sleeve for the plunger. This could explain the lower hydrogen values measured in the biscuit.

In order to reduce the gas porosity referred to v_{entrap} and v_{lubr}, and to increase the casting integrity, vacuum die-casting process has been successfully developed and deployed for commercial use in high volume production. This process exploits a controlled vacuum to extract gases from the die cavities, runner system, and shot sleeve during metal injection.[42]

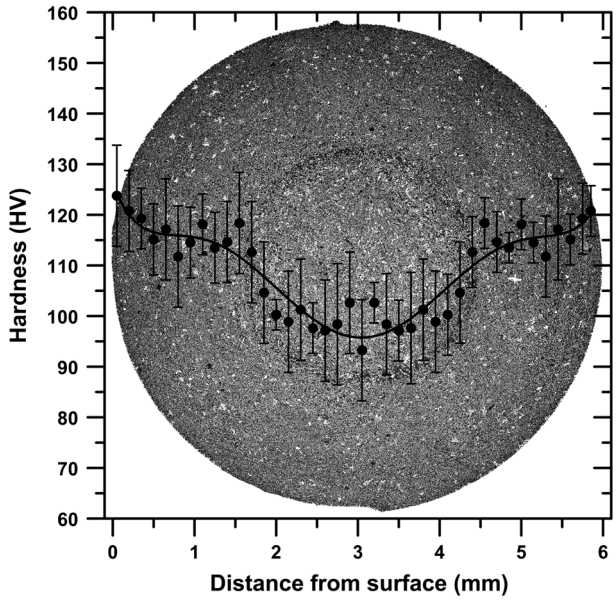

Fig. 15—Vickers microhardness profile over the entire cross section of the analyzed tensile bar in T1-condition; the standard deviations are given as error bars.

E. *Mechanical Testing*

1. *Hardness*

Figure 15 shows the Vickers microhardness profile of the analyzed AlSi9Cu3(Fe) tensile bar in T1-condition. The microhardness ranges between 95 and 125 HV, while the mean value is about 110 HV. The profile seems to reflect the local eutectic variations over the entire cross section of tensile bars with a general increase in the values from the casting center to the surface. There is evidence of a high peak in the region of ~1.6 mm from the surface of the castings, corresponding approximately to the central position of the inner segregation band previously estimated. Furthermore, higher microhardness values at the casting surface can be also due to higher supersaturation of atoms (Mg, Cu, Zn, and Si) in the α-Al matrix, which is referred to greater cooling rate in the regions in contact with the die wall.

2. *Tensile properties*

Figure 16 shows the engineering curves of die-cast (Ø6.0) and machined tensile bars (Ø3.4 and Ø3.0) in the T1-condition, while the average tensile data are reported in Table III. The crosses on the curves indicate the UTS and s_f of individual specimens, showing the range of results that can be expected from apparently similar specimens produced under constant casting conditions. In general, the reduction of the gage section of the specimens decreases the YS and UTS of the alloy, while the s_f increases by removing the surface layer enriched of brittle Al-Si eutectic.

The change of tensile strength and ductility seems to be ascribed to the variation of porosity content, eutectic fraction, and amount of brittle sludge compounds over the cross section of the casting. Reducing the gage

section, higher porosity concentration is obtained. The porosity locally reduces the load bearing area of the tensile specimen and results in the formation of an incipient neck with premature failure of the specimen. It has been demonstrated how the plastic properties of Al alloys decrease monotonically with increasing the area fraction of defects revealed on the fracture surfaces of tensile specimens.[14,43]

On the other side, for most cast Al-Si alloys, the tensile fracture can also be initiated by the cracking of eutectic silicon and brittle Fe-rich particles due to high tensile stresses induced by plastic deformation in the α-Al matrix. Cracked particles serve as nucleation sites for voids that eventually lead to fracture of the alloy. Therefore, higher concentration of eutectic silicon in the surface layer and coarse primary Fe-bearing compounds at the center act as weaker regions, facilitating voids' nucleation and fracture.

The initial YS of die-cast tensile specimens is largely determined by the relatively high supersaturation of atoms (Mg, Cu, Zn, and Si) in α-Al matrix and the fine-grained structure in the surface layer, which are both referred to the high cooling rate. Although the average grain size of in-cavity-solidified grains is almost uniform over the cross section, the greater amount of ESCs toward the center increases the average grain size.

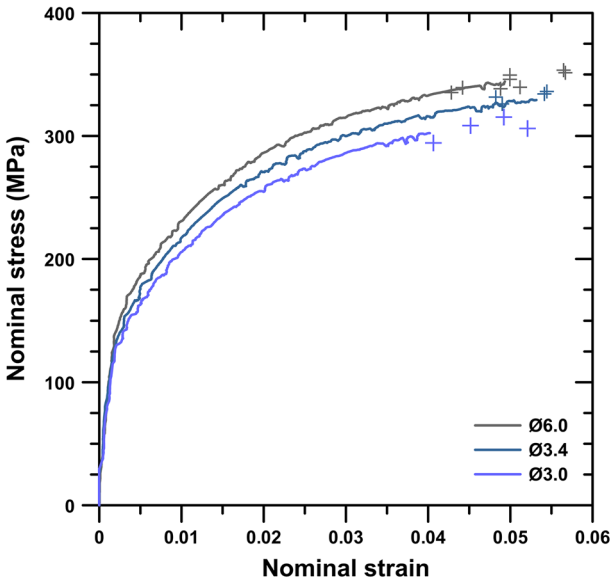

Fig. 16—Typical engineering stress/strain curves of die-cast (Ø6.0) and machined (Ø3.4, Ø3.0) AlSi9Cu3(Fe) tensile bars in T1-condition. The crosses indicate the failure point of some tested specimens.

Further, the ESCs are characterized by a different solidification history than in-cavity-solidified grains. As the ESCs have been the first to solidify in the shot sleeve, the alloying content of the ESCs is significantly less than the fine-grained structure in the surrounding matrix, as demonstrated in References 44.

Other mechanical properties such as the strain-hardening exponent n and the strength coefficient K (MPa), which are related to the true stress σ_{tr} (MPa) and the true plastic strain ε_{pl} according to the Hollomon equation

$$\sigma_{tr} = K\,(\varepsilon_{pl})^n, \qquad [5]$$

were analyzed (see Table III). The n and K values were determined using a double logarithmic plot of the true stress and the true plastic strain, where the n-value represents the slope and the K-value corresponds to the true stress at a true strain value of unity. The strength coefficient relates to the YS and strain-hardening exponent as[23]

$$K = \mathrm{YS}\left(\frac{E}{\alpha \cdot \mathrm{YS}}\right)^n, \qquad [6]$$

where E is the Young's modulus and α is a scale factor of order 1. No variation of the strain-hardening rate is here referred. Therefore, K becomes a sole function of the YS, which in turn is a matrix-controlled property. The values of E and α are ~71 GPa and 0.9, respectively.

Table III reports the values of the quality index Q (Eq. [3]) which, combining both strength and ductility, is believed to be more descriptive of the *true tensile properties* of castings than either the tensile strength or the elongation alone.[45] In general, Q decreases by reducing the gage section. Removing the surface layer, there is a decrease of 2 pct, while the further reduction from 3.4 to 3.0 mm, *i.e.*, machining also the region of the defect band, the quality index decreases of 11 pct. It has been stated how the presence of the surface layer potentially affects mechanical performance, corrosion properties, and pressure tightness of the whole cast component. This is critical for structural and safety HPDC components, such as automotive chassis parts, where very high ductility is a key mechanical requirement. In the present work, it seems that the main contribution of the surface layer on the mechanical properties of die-cast AlSi9Cu3(Fe) alloy concerns the yield point.

For structural applications, safety and reliability are, however, essential requirements. Several studies on cast metals have indicated how the Weibull distribution can reasonably describe the probability of fracture and the

Table III. Average Mechanical Properties of Die-Cast and Machined AlSi9Cu3(Fe) Tensile Bars in the T1-Condition

Gage Section (mm)	YS (MPa)	UTS (MPa)	s_f (Pct)	n	K (MPa)	Q (MPa)
Ø6.0	173 (3)	344 (7)	5.0 (0.5)	0.26 (0.01)	837 (14)	578 (21)
Ø3.4	160 (4)	333 (8)	5.3 (0.4)	0.26 (0.01)	805 (18)	566 (11)
Ø3.0	148 (5)	306 (8)	4.6 (0.4)	0.27 (0.01)	785 (25)	514 (21)

Standard deviation in parentheses.

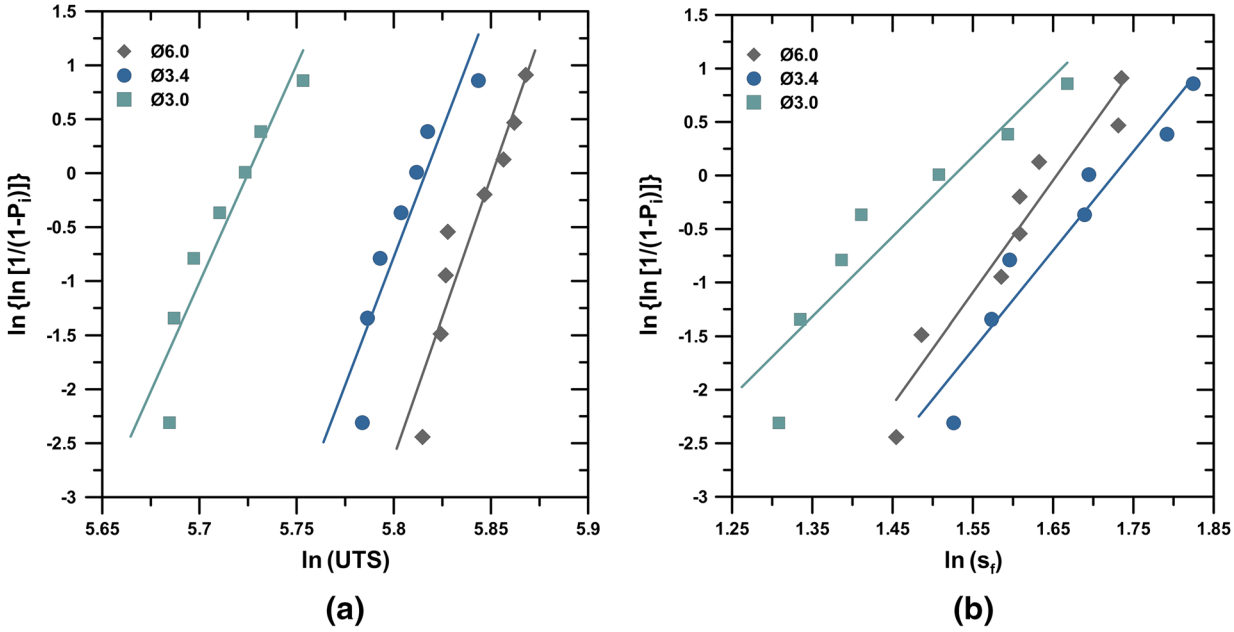

Fig. 17—Weibull plots of (*a*) UTS (in MPa) and (*b*) s_f (in pct) for die-cast and machined AlSi9Cu3(Fe) tensile bars in the T1-condition.

Table IV. Weibull Moduli, β, and Scale Parameters, η, for UTS and Elongation to Fracture Obtained from AlSi9Cu3(Fe) Tensile Specimens in the T1-Condition with Different Gage Sections

	UTS		s_f	
Gage Section (mm)	β	η (MPa)	β	η (pct)
Ø6.0	51.8	347	10.5	5.2
Ø3.4	47.4	335	9.3	5.6
Ø3.0	40.3	306	7.5	4.6

reliability of the casting.[24–26] The two-parameter form of the Weibull distribution was adopted

$$P_i = 1 - \exp\left[-\left(\frac{x}{\eta}\right)^{\beta}\right], \qquad [7]$$

where P_i is the cumulative fraction of specimen failures (in tensile test) estimated according the Benard method; x is the variable being measured (UTS or s_f); η is the scale parameter, *i.e.*, the characteristic stress (or strain) at which 63.21 pct of the specimens has failed; β is the shape parameter, alternatively referred to as the Weibull modulus. This modulus is a measure of the spread of the distribution and repeatability of the castings.

Figure 17 and Table IV show the Weibull plots and the corresponding quantitative results referred to the UTS and s_f of the analyzed tensile bars. It is clear from the Weibull moduli that the surface layer increases the reliability of the die-cast AlSi9Cu3(Fe) alloy, while the microstructural heterogeneities and the casting defects, concentrated at the center of the casting, reduce it. These findings seem to be in agreement with the results reported in Reference 46, which refers to AlSi7Mg gravity die-castings and where it is mentioned how the phenomenon of *skin effect* (referred as "*edge effect*" in Reference 46) clearly has a deep influence on the casting reliability.

IV. CONCLUSIONS

In the present work, detailed investigations have been carried out to document the salient microstructural heterogeneities and casting defects of a high-pressure die-cast AlSi9Cu3(Fe) alloy. These features are then addressed to the mechanical properties and reliability of separately die-cast tensile bars. The following conclusions can be drawn from the experimental results.

- Die-cast specimens consist of multiple positive segregations. Besides an inner eutectic segregation band, there exists a surface segregation and a general eutectic increase from the casting center to the surface.
- Externally solidified α-Al crystals, cold flakes, and sludge $Al_x(Fe,Mn,Cr)_ySi_z$ particles are even concentrated toward the casting center in a region defined by the segregation band. The concentration of ESCs is referred to increase the average grain structure of the die-cast material.

- Casting defects are mainly ascribed to gas porosity, whose formation originates from the decomposition of coolant and die lubrication in HPDC; these pores tend to be located toward the center of the cross section, enclosed by the segregation band. Contrary, there exists a surface layer, outside the defect band, that contains a low porosity content, and fine and uniform grain structure.
- The hardness profile seems to reflect the local eutectic variations in the casting.
- The progressively reduction of the gage section decreases the YS and UTS of the alloy, while the elongation to fracture increases by removing the *surface layer* outside the segregation band. However, machining also the region of the defect band, the ductility of the material decreases.
- The changes of tensile strength and ductility seem to be ascribed to the local variation of porosity content, eutectic fraction, and amount of brittle sludge compounds.
- From the Weibull statistics it is clear how the surface layer increases the reliability of the die-cast AlSi9-Cu3(Fe) alloy. This is a key mechanical requirement for the structural and safety HPDC components.

ACKNOWLEDGMENTS

This work was developed within the European Project MUSIC (MUlti-layers control & cognitive System to drive metal and plastic production line for Injected Components, FP7-FoF-ICT-2011.7.1, Contract No. 314145). The authors would like to acknowledge Raffineria Metalli Capra Spa (Brescia, Italy) for the financial support to the research and the skillful contribution of Toolcast Snc (Brugine, Italy) for high-pressure die-casting experiments.

REFERENCES

1. D.R. Gunasegaram, B.R. Finnin, and F.B. Polivka: *Mater. Forum*, 2005, vol. 29, pp. 190–95.
2. D.R. Gunasegaram, B.R. Finnin, and F.B. Polivka: *Int. J. Cast Met. Res.*, 2007, vol. 23, pp. 847–56.
3. M.R. Ghomashchi: *J. Mater. Process. Technol.*, 1995, vol. 52, pp. 193–206.
4. Z.-P. Guo, S.-M. Xiong, B.-C. Liu, M. Li, and J. Allison: *Metall. Mater. Trans. A*, 2008, vol. 39A, pp. 2896–2905.
5. M.R. Ghomashchi and G.A. Chadwick: *Met. Mater.*, 1986, vol. 2, pp. 477–81.
6. M.S. Dargusch, G. Dour, N. Schauer, C.M. Dinnis, and G. Savage: *J. Mater. Process. Technol.*, 2006, vol. 180, pp. 37–43.
7. S. Otarawanna, H.I. Laukli, C.M. Gourlay, and A.K. Dahle: *Metall. Mater. Trans. A*, 2010, vol. 41A, pp. 1836–46.
8. Z.W. Chen: *Mater. Sci. Eng. A*, 2003, vol. 348A, pp. 145–53.
9. S. Otarawanna, H.I. Laukli, C.M. Gourlay, and A.K. Dahle: *Mater. Chem. Phys.*, 2011, vol. 130, pp. 251–58.
10. C.M. Gourlay, H.I. Laukli, and A.K. Dahle: *Metall. Mater. Trans. A*, 2007, vol. 38A, pp. 1833–44.
11. H.I. Laukli, O. Lohne, S. Sannes, H. Gjestland, and L. Arnberg: *Int. J. Cast Met. Res.*, 2003, vol. 16, pp. 515–21.
12. H.I. Laukli, C.M. Gourlay, and A.K. Dahle: *Metall. Mater. Trans. A*, 2005, vol. 36A, pp. 805–18.
13. S. Otarawanna, C.M. Gourlay, H.I. Laukli, and A.K. Dahle: *Metall. Mater. Trans. A*, 2009, vol. 40A, pp. 1645–59.
14. G. Timelli: *Metal Sci. Technol.*, 2009, vol. 28, pp. 9–17.
15. G. Timelli and F. Bonollo: *Mater. Sci. Eng. A*, 2010, vol. 528A, pp. 273–82.
16. M. Conserva: *Diecasting Foundry Tech.*, 2013, vol. 8, pp. 28–29.
17. EN 1706:2010, Aluminium and Aluminium Alloys—Castings—Chemical Composition and Mechanical Properties, European committee for standardization, pp. 24–25.
18. M.E. Schlesinger: *Aluminum Recycling*, 1st ed., CRC Press, Boca Raton, 2007, pp. 1–8.
19. G. Timelli, F. Grosselle, F. Voltazza, and E. Della Corte: *Proc. International Conference High Tech Die Casting*, Montichiari, Italy, Paper No. 35, April 9–10, 2008.
20. M.M. Makhlouf, D. Apelian, and L. Wang: *Microstructure and Properties of Aluminium Die Casting Alloys*, 1st ed., North American Die Casting Association, Rosemont, IL, 1998, p. 68.
21. ASTM E384-11e1, Standard Test Method for Knoop and Vickers Hardness of Materials, ASTM International, West Conshohocken, PA, 2011.
22. UNI EN ISO 6892:2009, Metallic Materials: Tensile Testing: Part 1: Method of Test at Room Temperature, European Committee for Standardization, pp. 1–65.
23. C.H. Cáceres: *Int. J. Cast Met. Res.*, 1998, vol. 10, pp. 293–99.
24. W. Weibull: *J. Appl. Mech.*, 1951, vol. 18, pp. 293–97.
25. X. Teng, H. Mae, and Y. Bai: *Mater. Sci. Eng. A*, 2010, vol. 527A, pp. 4169–76.
26. N.R. Green and J. Campbell: *Mater. Sci. Eng. A*, 1993, vol. 173A, pp. 261–66.
27. M.C. Flemings: *Metall. Trans. A*, 1991, vol. 22A, pp. 957–81.
28. S. Khan and R. Elliott: *J. Mater. Sci.*, 1996, vol. 31, pp. 3731–37.
29. S. Ferraro, G. Timelli, and A. Fabrizi: *Mater. Sci. Forum*, 2013, vol. 765, pp. 59–63.
30. S.G. Shabestari: *Mater. Sci. Eng. A*, 2004, vol. 383A, pp. 289–98.
31. M.V. Kral: *Mater. Lett.*, 2005, vol. 59, pp. 2271–76.
32. C.M. Gourlay and A.K. Dahle: *Nature*, 2007, vol. 445, pp. 70–73.
33. B. Meylan, S. Terzi, C.M. Gourlay, M. Suéry, and A.K. Dahle: *Scripta Mater.*, 2010, vol. 63, pp. 1185–88.
34. S. Otarawanna, C.M. Gourlay, H.I. Laukli, and A.K. Dahle: *Mater. Charact.*, 2009, vol. 60, pp. 1432–41.
35. H.I. Laukli, C.M. Gourlay, A.K. Dahle, and O. Lohne: *Mater. Sci. Eng. A*, 2005, vol. 413–414A, pp. 92–97.
36. D.M Stefanescu: *Science and Engineering of Casting Solidification*, 2nd ed., Springer-Verlag GmbH, Heidelberg, 2009, pp. 60–63.
37. S.G. Lee, G.R. Patel, and A.M. Gokhale: *Scripta Mater.*, 2005, vol. 52, pp. 1063–68.
38. A.K.M. Aziz Ahamed, H. Kato, K. Kageyama, and T. Komazaki: *Mater. Sci. Eng. A*, 2006, vol. 423A, pp. 313–23.
39. S. Sannes and H. Westengen: *Proc. Int. Conf. on Magnesium Alloys and Their Applications*, B.L. Mordike and K.U. Kainer eds., Werkst-off-Informationgesellschaft, Frankfurt, Germany, 1998, pp. 223–28.
40. M. Warmuzeka, W. Ratuszekb, and G. Sęk-sas: *Mater. Charact.*, 2005, vol. 54, pp. 31–40.
41. G. Timelli, S. Ferraro, and A. Fabrizi: *Int. J. Cast Met. Res.*, 2013, vol. 26, pp. 239–46.
42. E.J. Vinarcik: *High Integrity Die Casting Processes*, 1st ed., John Wiley & Sons, New York, 2003, pp. 7–10.
43. C.H. Cáceres and B.I. Selling: *Mater. Sci. Eng. A*, 1996, vol. 220A, pp. 109–16.
44. H.I. Laukli, A. Graciotti, O. Lohne, H. Gjestland, and S. Sannes: *NADCA Trans.*, 2002, vol. 21, pp. 1–4.
45. N.D. Alexopoulos: *Mater. Des.*, 2007, vol. 28, pp. 534–43.
46. X. Dai, X. Yang, J. Campbell, and J. Wood: *Mater. Sci. Technol.*, 2004, vol. 20, pp. 505–13.